J Clust Sci (2015) 26:1153–1170
DOI 10.1007/s10876-014-0804-3

ORIGINAL PAPER

Meissner Effect in Ultra-Dense Protium p($l = 0$, $s = 2$) at Room Temperature: Superconductivity in Large Clusters of Spin-Based Matter

Leif Holmlid · Stephan Fuelling

Received: 22 May 2014Published online: 12 October 2014

Abstract Ultra-dense protium p($l = 0$) is superfluid at room temperature, as is its more often studied deuterium counterpart D($l = 0$). p($l = 0$) can be deposited on surfaces by a source which produces a stream of clusters. A magnetic field strongly influences the type of clusters formed. Very little of chain clusters of p($l = 0$) and the closely related form p($l = 1$) exists on the magnet surface or within 0.5 mm from the magnet surface. The removal of the p($l = 0$) and p($l = 1$) entity in strong magnetic fields is due to a Meissner effect as in the case of D($l = 0$). Contrary to the case of D($l = 0$), small symmetric p($l = 0$) clusters formed by 3 and 4 hydrogen atoms are not left on the magnet pole face when the large chain-clusters lift in the magnetic field. Symmetric p_4($l = 0$) clusters are unlikely since four fermions cannot interact in this way. Instead, p_2 pairs are included as bosons in the chain cluster structure as observed previously.

Keywords Ultra-dense protium · Superconductor · Coulomb explosion · Magnetic field

Introduction

Ultra-dense deuterium D($l = 0$) has been studied using laser-induced Coulomb explosions and fragmentation of the clusters forming this material [1–4]. (For changes in notation, see below in the theoretical section). It was shown to be

L. Holmlid (✉)
Division of Atmospheric Science, Department of Chemistry, University of Gothenburg, 412 96 Göteborg, Sweden
e-mail: holmlid@chem.gu.se

S. Fuelling
Department of Physics, University of Nevada Reno, 1664 N. Virginia Street, Reno, NV 89557-0220, USA

superfluid [5] and to give a Meissner effect [6], thus a lifting of the clusters in a static magnetic field. The density of the material is up to 10^{29} cm^{-3}, corresponding to a theoretical D–D distance of 2.23 pm [7] and an experimental distance of 2.3 ± 0.1 pm [1–4]. A dense deuterium phase was predicted by Berezhiani et al. [8] to have both superfluid and superconducting properties. The material consists of chain clusters D_{2N}, with D–D pairs rotating around the cluster axis, which presumably is also the location of a quantum vortex [9, 10]. The quantum mechanical basis for D($l = 0$) was further discussed by Winterberg [11, 12], pointing out the resemblance to other superfluids [13]. D($l = 0$) forms films on metal surfaces, but does not give condensation on polymer surfaces [14]. A similar material formed from protons, called ultra-dense protium p($l = 0$), was recently shown to exist [15, 16]. It has a slightly different structure than D($l = 0$) and contains also proton pairs which partially replace the deuterons in the D_{2N}-like basic cluster structure [16]. The detailed structure of ultra-dense materials was recently further studied [7]. It was shown to be based on the electron spin, giving different interatomic distances depending on the value of a spin quantum number s. This quantum number was identified experimentally to have values $s = 1$, 2 or 3, giving an interatomic distance of only 0.57 pm in level $s = 1$ [7]. Here, the methods used in the Meissner study of D($l = 0$) [6] are now applied to p($l = 0$) with a few improvements in the techniques used.

Theory

Rydberg Matter (RM) based on the electron orbit angular momentum l was predicted around 1980 [17, 18] and has been studied for a long time [19]. A recent review exists [20]. Such cluster-forming materials for hydrogen are indicated as H($l = 1$), H($l = 2$) etc. where H(l) in short form may indicate either protium p(l) or deuterium D(l). This position of the symbols is in agreement with the normal convention to indicate the electronic state within parenthesis after the atomic or molecular symbol. Recently, RM based on the spin angular momentum s has been described and observed [7], so far with values of $s = 1$, 2 and 3. This type of matter is usually called ultra-dense hydrogen with notation as H($l = 0$) for simplicity, with most studies concerned with the level $s = 2$ with experimental H–H bond distance of 2.3 ± 0.1 pm [1–4]. Thus, the full notation of such a type of material (or cluster) is H($l = 0$, $s = 2$). The previously used notation H(−1) (which indicated the presumed "inverted" state of the ultra-dense material [1]) is now replaced with the more correct H($l = 0$) or H(0) in short form. Most reports of ultra-dense hydrogen have in fact studied ultra-dense deuterium D($l = 0$) due to its slightly simpler structure, with less interaction between the nuclei due to their Boson properties. A theoretical description of D($l = 0$) was recently given by Winterberg. This stresses the similarity to other superfluids [11, 12].

When a laser pulse passes through an ultra-dense material or other RM materials, the photons may excite (displace) a few electrons so that two ions become exposed to each other. Coulomb explosions (CE) then force the ions to move apart rapidly, in <1 fs for H($l = 0$). When CE takes place, the ions fly apart with almost all their

repulsion energy as kinetic energy release (KER) in the ionic fragments. It is then possible to determine the initial repulsion energy between the ions by measuring the kinetic energy of the fragments at a large distance from the explosion event. The distance between the ions before the CE is found directly from the Coulomb formula as

$$r = \frac{1}{4\pi\varepsilon_0}\frac{e^2}{E_{kin}} \tag{1}$$

where ε_0 is the vacuum permittivity, e the unit charge on the fragment ions and E_{kin} the sum kinetic energy for the fragments (KER) from the CE. The fraction of the KER that is observed on each fragment depends on the mass ratio of the fragments. The kinetic energy is determined most easily by measuring the time-of-flight (TOF) of the fragments and then converting this quantity to kinetic energy. This requires that the mass of the particle is known, which is simplified when working with hydrogen. Spin level $s = 2$ gives a theoretical H–H distance of 2.23 pm [7]. $s = 1$ gives a H–H distance of 0.57 pm, while $s = 3$ has 5.0 pm [16].

The energy level of H($l = 0$) is lower than that of H($l = 1$). The interconversion between H($l = 1$) and H($l = 0$) is relatively rapid [21]. It often shows an oscillatory behavior in time [2]. Numerous studies of the clusters of H($l = 0$) show that they are chain clusters of the form H_{2N} with N an integer. This form is shown in Fig. 1. Each "bead" is formed by a pair H–H which rotates around their common mass-center. Several H–H pairs form the chain clusters. The electrons may form a vortex in each long cluster. Each such cluster may show a Meissner effect. In the superconducting state some electrons have orbits with large dimensions, as described by Hirsch [22]. The superconducting state thus corresponds to a state with orbiting electrons. This is similar to an ordinary RM cluster state with $l > 0$, but with the plane of the orbit given by the magnetic field direction, not by the geometry of the cluster as in the case of an ordinary (orbital angular momentum-based) RM cluster. Small clusters like H_3 and H_4 [4] may not be able to support a preferential direction of the cluster or a vortex. Thus, they will probably not show a Meissner effect. Such non-floating clusters were observed in the case of D($l = 0$) [6]. However, they are not likely to be formed easily in the present case with ultra-dense protium p($l = 0$) due to the Fermion character of the protons.

The process of lifting of the superconducting clusters in the magnetic field was described previously [6]. It is assumed that the superconductive current in the large D($l = 0$) clusters forms a circular loop, to simplify the calculation of the magnetic moment in the cluster. This is in agreement with the large electron orbits proposed to exist in type-II superconductors [22]. Formulas were derived for the cluster balancing height above the center of the magnet. However, we here repeat only the formulas derived for the radius of the electron orbit r in a general one-atom part of the cluster with mass m. This is found from theory as

$$r = \left(\frac{2\pi\mu_0 mgz^7}{3B_0^2V_M^2}\right)^{1/3} \tag{2}$$

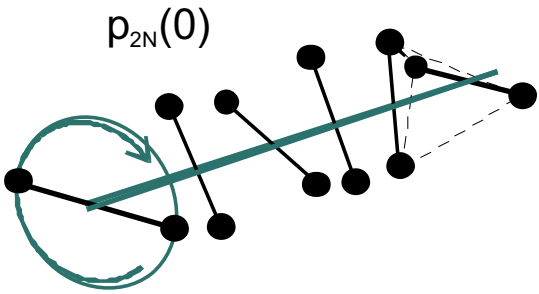

Fig. 1 Shape of the chain or "bead" clusters forming the superconductive phase p($l = 0$). In the superconductive state, some electrons orbit around the cluster

where μ_0 is the vacuum permeability, g is the acceleration of gravity, z is the distance from the center of the magnet, B_0 is the magnetic field close to the pole face of the magnet, and V_M is the total volume of the magnet.

For a real small permanent magnet, the variation of B with distance is different from the simple theoretical form assumed in the derivation of Eq. (2). It is possible to model the magnetic field on the centerline of a cylindrical magnet as described previously [6]. If the field strength $B(z)$ and its derivative with distance $B'(z)$ can be found, the radius of the electron orbit r in a general one-atom part of the cluster is found as

$$r = \left(\frac{\mu_0}{2\pi}\frac{mg}{B(z)B'(z)}\right)^{1/3} \tag{3}$$

For realistic values of the magnetic field, values of r were found to be a few pm with the distance $z = 1.5$ mm (half the magnet thickness) [6]. Thus, r is in good agreement with the size of the subunits in the ultra-dense hydrogen, ranging from 0.57 to 5.0 pm for the three spin levels [7].

Experimental

The apparatus has been described in several publications, for example in [10]. It has a base pressure of $<1 \times 10^{-6}$ mbar and is shown in Fig. 2. The central source part is described in Ref. [3]. The emitter is a cylindrical (extruded) sample of an industrial iron oxide catalyst doped with K (initially at 8 wt%) [23, 24], a so called styrene catalyst type Shell S-105 (no longer produced). This type of catalyst is an efficient hydrogen abstraction and transfer catalyst. The emitter is mounted in the tight-fitting opening of a metal tube. This source metal tube is heated by an AC current through its wall up to 400 K. Hydrogen gas (99.9995 % pure) is admitted through the tube at a pressure up to 1×10^{-5} mbar in the chamber.

The magnetic field is produced by a NdFeB magnet (SSG N33SH) with dimensions $3 \times 4 \times 8$ mm^3. The magnetic field strength is 0.17 T at 1.0 mm distance from the pole face (the largest surface), with residual magnetic field of 1.1 T according to the manufacturer. Two different set-ups are used, as shown in

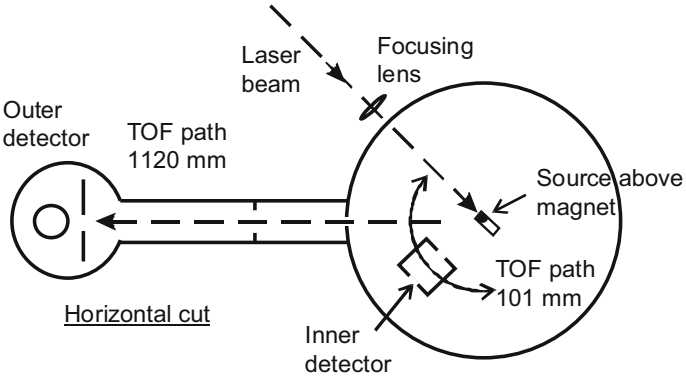

Fig. 2 Horizontal cut through the apparatus. Both the inner and outer detectors have been used

Fig. 3. In one type of experiment (a) the magnet lies on a horizontal surface and the laser beam passes above the magnet parallel to the magnet pole face, or hits one of the vertical surfaces. In this case, another identical magnet was mounted below the support table to hold the top magnet in place, probably giving a slightly stronger magnetic field close to the top magnet than given by the manufacturer. The field strength has also been measured with a Hall effect sensor (Allegro A1326 giving 2.5 mV G^{-1}) in this type of experiment. The field strength at a distance of 4 mm from the pole of the magnet was 470 G, and at 3 mm distance 900 G. This agrees roughly with manufacturer's data. The magnet is located on a small horizontal table approximately 1 cm below the source, to allow the p($l = 0$) material formed in the catalyst to drop down on the table and on the magnet pole face. p($l = 0$) is superfluid [13] and creeps over the surface and also over the raised rim of the table. At this outer edge surface, the magnetic field strength is low and the signal from this edge is used for comparison purposes. The second type of experiment shown as (b) in Fig. 3 has the magnet at approximately 45° to the horizontal. On top of it, touching the pole face, a 0.25 mm thick Ta foil resides, which covers the magnet and the sloping support part. The laser is moved from on top of the magnet to the position with no magnet below the foil as shown in (b) in Fig. 3.

A Nd:YAG laser with an energy of <125 mJ in 5 ns long pulses at 10 Hz is used at 532 nm. The laser beam is focused at the center of the chamber with an $f = 400$ mm spherical lens. The lens is mounted in a vertical motion translation stage which allows the laser beam to be shifted controlled distances down to a few m. The intensity in the beam waist of (nominally) 70 m diameter is relatively low, $\leq 10^{12}$ W cm^{-2} as calculated for a Gaussian beam. Two different dynode-scintillator-photomultiplier detectors which measure the TOF spectra of the neutral and ionized flux from the laser initiated processes are shown in Fig. 2. The inner detector can be rotated around the center of the chamber and is here used at 45° and 70° relative to the incoming laser beam. The fast particles impact on a steel catcher foil in the detector, and fast ions ejected from there are drawn towards a Cu–Be dynode held at −7.0 kV inside the detector. The total effective flight distance for the ions from the

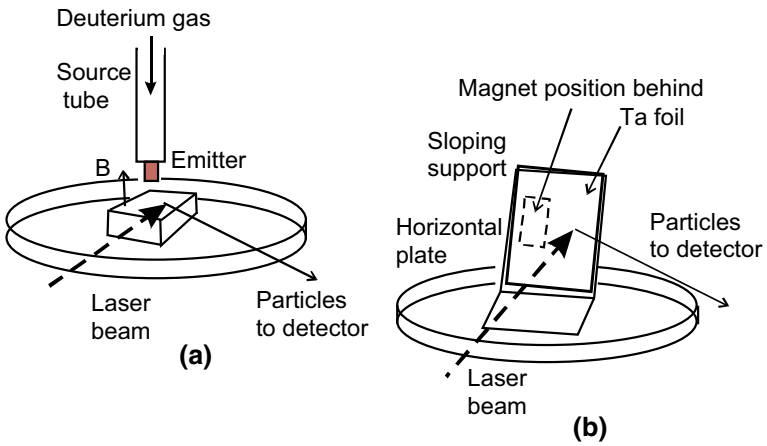

Fig. 3 The two set-ups used for the magnet. The source not included in (**b**) for simplicity sits above the Ta foil. The two positions of the laser in the (**b**) experiment are on the foil covering the magnet and on the foil with no magnet below the foil as shown

laser focus to the catcher foil is 101 mm by direct measurement and internal calibration [1, 21]. The photomultiplier (PMT) is Electron Tubes 9128B with single electron rise time of 2.5 ns and transit time of 30 ns. This PMT is covered by Al foil and black plastic tape giving only a small active cathode area of 2–3 mm^2, to avoid saturation. The outer detector is at a longer flight distance of 1120 mm. It is fixed at an angle of 45º relative to the laser beam. This detector has no catcher foil but the field from the dynode at −5 kV instead draws the ions into the detector. The PMT is Electron Tubes 9813B with single electron rise time of 2 ns and transit time of 46 ns. Blue glass filters in front of the PMTs remove the signal from the laser light. A fast preamplifier (Ortec VT120A, gain 200, bandwidth 10–350 MHz) is used. The signal from the PMT is normally collected on a fast digital oscilloscope (Tektronix TDS 3032, 300 MHz), sometimes using the digital averaging mode in the oscilloscope. A multi-channel scaler (MCS) with 5 ns dwell time per channel is also used (EG&G Ortec Turbo-MCS). Each spectrum consists of the sum from 300 to 1,000 laser shots.

Results

The results of the Meissner effect for p(0) are quite similar to those of D(0) [6]. This means that only a few pertinent results are reported here. The main experimental setup has been improved relative to the D(0) Meissner study [6] by using a precise shifting of the focusing lens for the laser beam instead of a shifting of the laser beam by rotation of a glass plate in the beam, and by using the outer detector with a long flight path, and thus decreased risk of signal saturation and shock-wave reflections. The inner detector has also been rotated away from the point of laser impact to just observe the signal from the layer on top of the magnet, hiding the signal from the

direct hit of the laser beam. The main tests presented here for the Meissner effect are the lifting of the coupled forms p(1) and p(0) over the pole face of the magnet, as depicted in Fig. 3(a). Also the observation of p(2) as the lowest excitation level of p (RM) in the magnetic field is similar to the case of D(2), reported in [6]. The experiment with sloping support and sampling on a foil with or without magnet below the foil which was used in [6] is also done for p(0) here as in Fig. 3(b) to simplify the direct comparison of the results. This shows that the Meissner effect is weaker for p(0) than for D(0). Finally, the structure of the small p(0) clusters that exist on the magnet surface is investigated using the setup in Fig. 3(a), showing different cluster properties and fragmentation behavior than in the case of D(0).

Horizontal Magnet

The main effects of the magnet are shown in Fig. 4 where pulse-counting in the MCS has been used due to better pulse response. The signal found at the edge of the magnet [Fig. 3(a)] is composed of a few different regions in space along the laser beam with varying density and composition, while the two other signals shown are of a spatially more homogeneous nature. The long signal tail above 10 s may of course contain contributions from several excitation levels p(l), but for the result above the magnet pole face, only p(3) and p(4) seem to contribute substantially. However, the intensity at long times above the magnet pole face is not larger than any of the other signals. This indicates no lifting of clusters of the excitation levels p (3) and p(4) in the magnetic field. Thus, only the coupled levels p(0) and p(1) lift in the magnetic field, in the same way as shown by the Meissner effect in D(0) [6].

The variation in concentration of large clusters of p(0) and p(1) above the magnet pole face is shown directly in Fig. 5. At a distance of 0.4 mm above the pole face, the signals due to p(0) and p(1) are relatively large, while lower close to the surface, both p(1) and most clearly p(0) decrease strongly. At almost all the locations shown, the level p(2) seems to exist, and the level p(1) is depleted. The variation of the signal with the location of the laser focus above the pole face of the magnet [at higher p(0) densities], at the end face of the magnet and on the rim of the supporting table is shown in Fig. 6. Two of these positions (end face and rim of table) are at lower magnetic field strength than those in Fig. 5. Thus, small p(0) clusters and high intensities of large p(0) clusters exist there. The most intriguing effect in Fig. 6 may be that the level p(2) is only observed above the magnet surface since p(1) and p(0) are the lowest levels occupied which means that the clusters have fallen down to these low-lying levels in the two other measurements. [The intensity at 50–60 s above the pole face could also be due to fragments with mass 5 from p(1)]. A comparison shows that p(2) is probably abundant in the strong magnetic field above the pole face in Fig. 5, while the p(1) signal is much lower than in Fig. 6.

As also noted in [6], the TOF spectra may depend strongly on the measurement procedure, for example the spectrum from the first laser pulse may be different (larger or smaller) than when the laser has been running for a duration of 30 s or so. An example is given in Fig. 7, where it is clearly shown that this effect is strong in the cluster cloud above the magnet pole face, while it is weaker closer to the surface.

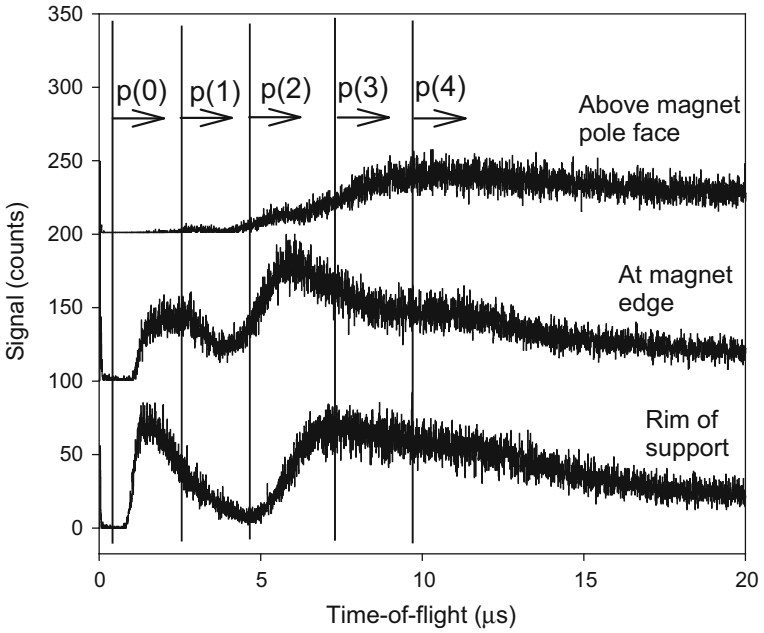

Fig. 4 Main effects of the magnet on the neutral p(RM) cluster distributions using the setup in Fig. 3(a). Above the magnet in the strong field, levels p(0) and p(1) are depleted relative to the layers at the edge of the magnet and the rim of the support table. TOF limits are given in Table 1. Inner detector at 70°, 300 laser shots

Table 1 The shortest possible TOF for p (repelled from infinite mass) from asymmetric CE processes with 2 and 3 charges in the p(RM) clusters, with 101 and 1,120 mm flight paths to the detectors

Excitation level	Inner detector 101 mm		Outer detector 1,120 mm	
	CE 2+	CE 3+	CE 2+	CE 3+
p(0)	291 ns		3.2 μs	
p(1)	2.4 μs	1.7 μs	26.4 μs	18.7 μs
p(2)	4.8 μs		52.8 μs	
p(3)	7.2 μs		79.4 μs	
p(4)	9.5 μs		106 μs	

This effect is here apparently due to the time required for replenishment of the upper parts of the cluster cloud in the magnetic field. This process probably involves formation of large clusters on the surface and lifting of the clusters in the magnetic field to a distance of 0.5–1.0 mm from the pole face. In the lower panel in Fig. 7 with the first laser pulse only (indicated as laser start), the increase in p(0) density with height above the magnet pole face is observed as in Fig. 5. However, small clusters of p(1) have low density also initially, not only with the laser running as shown in the upper panel in Fig. 7.

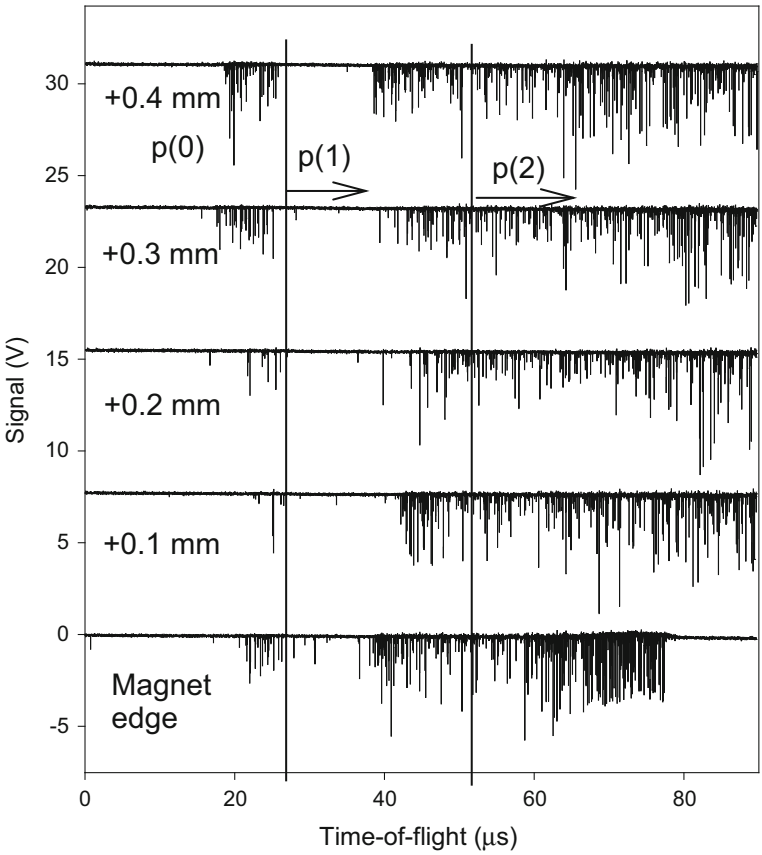

Fig. 5 One experiment with probing for neutral clusters above the pole face of the magnet, at high magnetic field strength, using the setup in Fig. 3(a). Outer detector, single-shot spectra, laser running. The intensity of p($l = 0$) clusters is lowest at 0.1–0.2 mm above the surface, which means that such clusters have lifted in the magnetic field

Sloping Magnet

Further results confirming these points are found with the sloping magnet setup in Fig. 3(b). Results are shown in Fig. 8 using the inner detector and in Fig. 9 with the outer detector. A large difference is found in the spectra observed from the layer on the Ta surface above the magnet and above the position with no magnet below the foil, with much less intensity of p(0) and small p(1) clusters with the magnet underneath. In this type of experiment, the total layer on top of the surface is sampled by the laser, and when p(0) is not observed on top of the magnet (covered by the Ta foil), this means that p(0) clusters do not exist in the field. Thus they are clearly not stable in the magnetic field. These results can be compared with the results on D(0) in [6] using the same setup (in Fig. 7 in [6]). Such a comparison

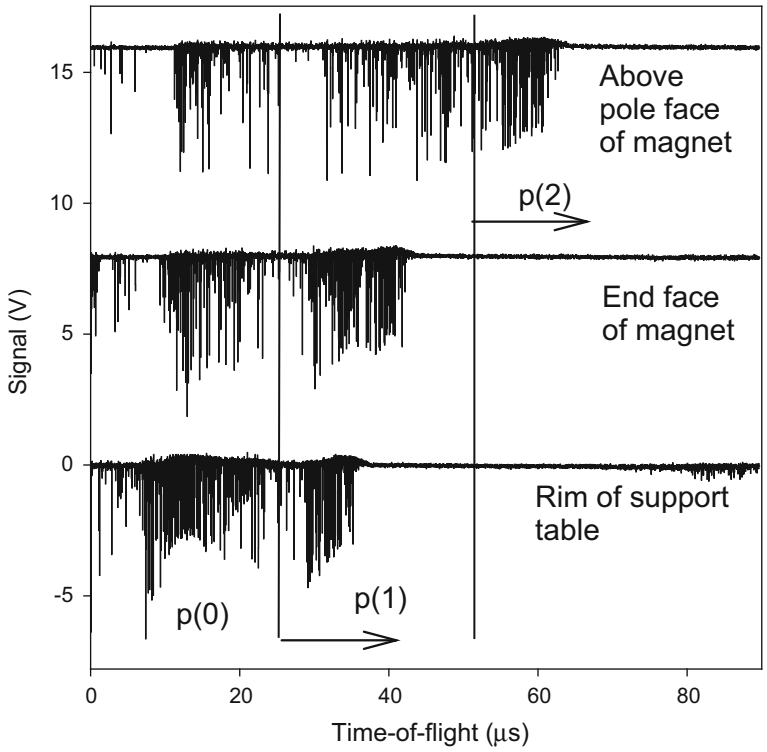

Fig. 6 One experiment with comparison of neutral cluster signals above the magnet, at the vertical end face of the magnet and at the outer rim of the support table, using the setup in Fig. 3(a). Outer detector, single-shot spectra, laser running. p($l = 0$) is clearly depleted in the strong magnetic field above the pole face, and the level p($l = 2$) is occupied

shows that the influence of the magnetic field is weaker for p(0) than for D(0), indicating a weaker Meissner effect for p(0).

Small Clusters With Horizontal Magnet

In the case of D(0) [6], the signal due to small clusters of the types D_3 and D_4 is large also at the magnet surface. For p(0), this is not the case and the signal due to small p(0) clusters is always small, even on the end face of the magnet at relatively low magnetic field strength. This indicates that small clusters p_3 or p_4 either are less stable than D_3 and D_4, or that they have magnetic dipoles and thus also lift in the magnetic field and do not stay on the surface. The results in Figs. 8 and 9 indicate that small p(0) clusters do not float in the field, since they are not observed at all above the magnet. Using MCS pulse counting with the inner detector, the spectrum in Fig. 10 is found at the end face of the magnet with the setup in Fig. 3(a). It shows the fastest particles ejected from p(0). A few different distributions seem to exist in this first peak, but the main peak is close to fragmentation of p_2 to two p, each with

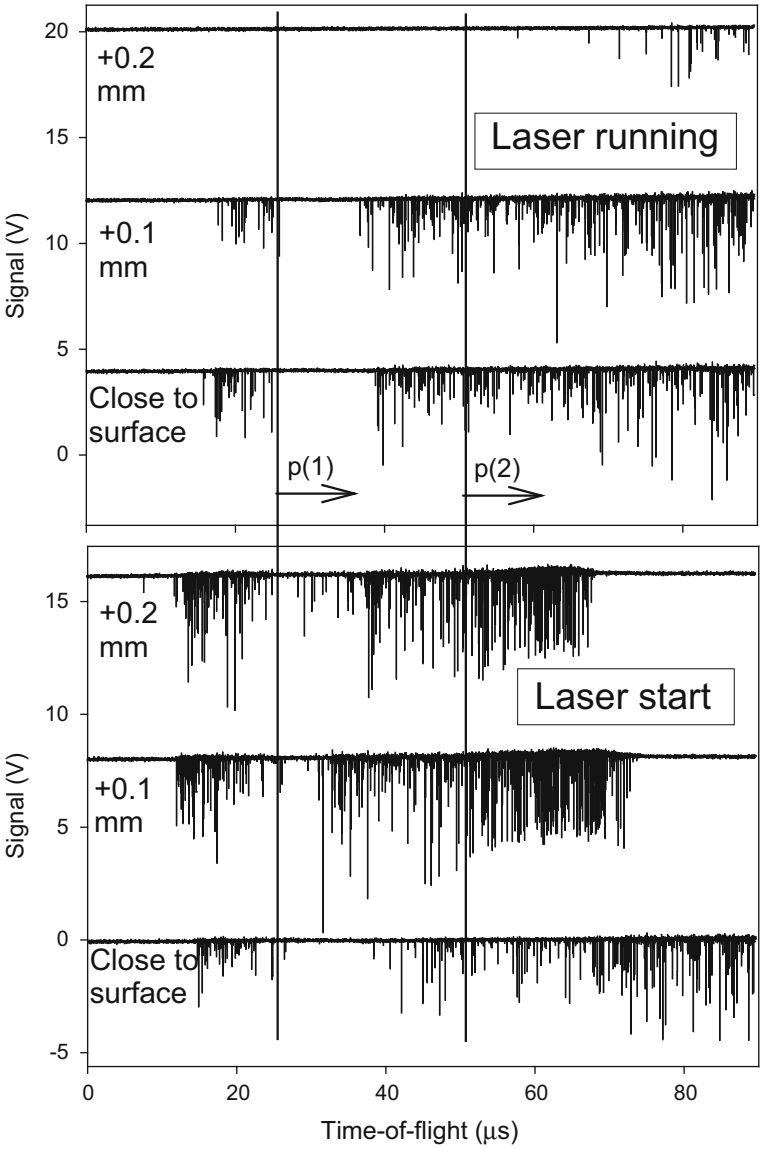

Fig. 7 One experiment showing the effect of laser depletion of the neutral cluster cloud lifted above the pole face, using the setup in Fig. 3(a). Laser start means the first single-pulse shot, laser running means single-shot measurement with laser running at 10 Hz. Outer detector, single-shot spectra

315 eV arriving at 411 ns according to Table 2. The fastest signal observed in Fig. 10 has a TOF as short as 203 ns, which is lower than any value in Table 2. It corresponds to a limiting value for fragmentation of spin level $s = 1$ for p(0), with a p–p distance of 0.56 pm [7]. A fragmentation $p_2^+ \longleftrightarrow p_N^+$ will give a TOF of 203 ns to the inner detector, in good agreement with the observed rise of the signal in

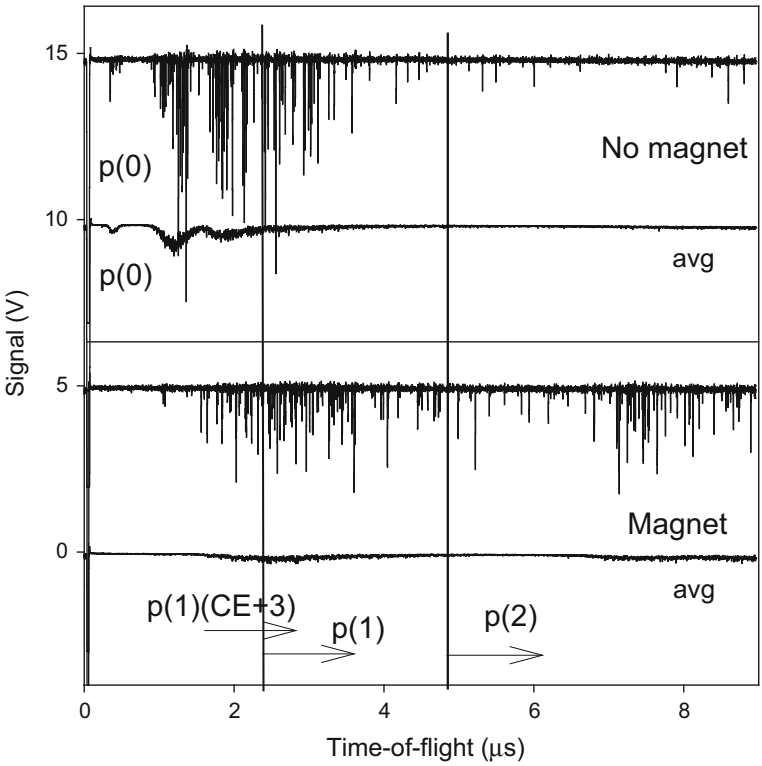

Fig. 8 Magnet comparison experiment as shown in Fig. 3(b), with inner detector at 45° relative to laser beam. Single-shot signals with laser running, and average signals (avg). The shortest TOF limits from Table 1 are indicated. Note the small signal for p($l = 0$) and also for p($l = 1$) on the magnet. The level p ($l = 2$) shows greater intensity on the magnet

Fig. 10. The theoretical KER for this level is 2586 eV. Note that this process involves a dimer ion p_2^+.

Further experiments with the inner detector giving higher intensities of the fast peaks for p(0) are shown in Fig. 11. With the setup in Fig. 3(a), the side of the magnet facing the detector, right below the source, is there tested with the laser, at relatively low magnetic field strength but high laser intensity. Both pulse-counting and averaged oscilloscope results are shown to give the full picture. The intensity seems to be due to both $p^+ \longleftrightarrow p_N^+$ and $p_2^+ \longleftrightarrow p_N^+$ fragmentations, from the spin levels $s = 1$ and $s = 2$ [7]. The limits of the TOF for the inner detector are given in Table 3, corresponding to the vertical lines in Figs. 10 and 11. The p_2 ejecting processes are due to the pairs of protons in the p(0) clusters, first observed in [16]. This could be the first observation of the spin level $s = 1$ for p(0) (however, see further in the "Discussion" section). Spin level $s = 1$ was previously identified for D (0) [7].

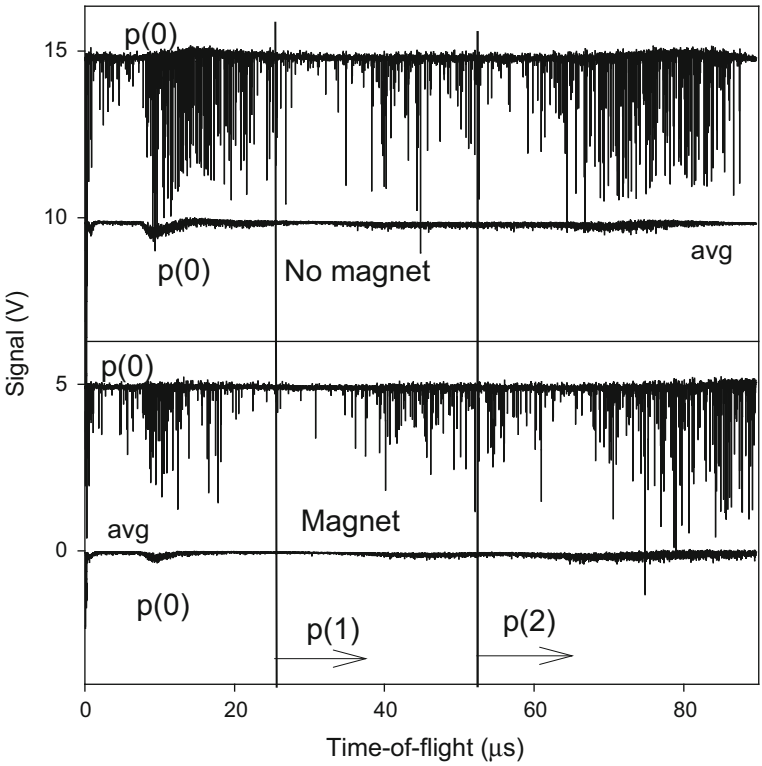

Fig. 9 Magnet comparison experiment as shown in Fig. 3(b), with outer detector. Single-shot signals with laser running, and average signals (avg). The shortest TOF limits from Table 1 are indicated. Note the small signal for p($l = 0$) and also for p($l = 1$) on the magnet

Discussion

A comparison with the results for the Meissner effect in D(0) indicates that the effects observed are smaller for p(0) than for D(0). This may be most clearly seen by comparing Fig. 7 in [6] with Fig. 8 here. This is not unlikely, since the structure of p(0) is more complex than that of D(0) [16]. The pairing of protons to boson particles p_2 certainly gives a more complex structure than the ideal one shown in Fig. 1. This may mean that the material p(0) has a lower temperature of transition from a superconductor than D(0). D(0) is better organized than p(0), as can be seen from laser fragmentation spectra [10]. A disturbed structure should give a lower transition temperature, since clusters with a complex p_2–p pair (or triad) structure instead of p–p for the cluster "beads" may act as a normal component [6, 13] with no super properties. If this is the case, the heating by the laser impact may be sufficient to make the material non-superconductive with no lifting in the magnetic field.

One intriguing point to discuss is the possibility that ordinary RM clusters [20] may show a Meissner effect. Such clusters are normally planar with strong magnetic dipoles perpendicular to the cluster plane [20]. Of course, they have rotational

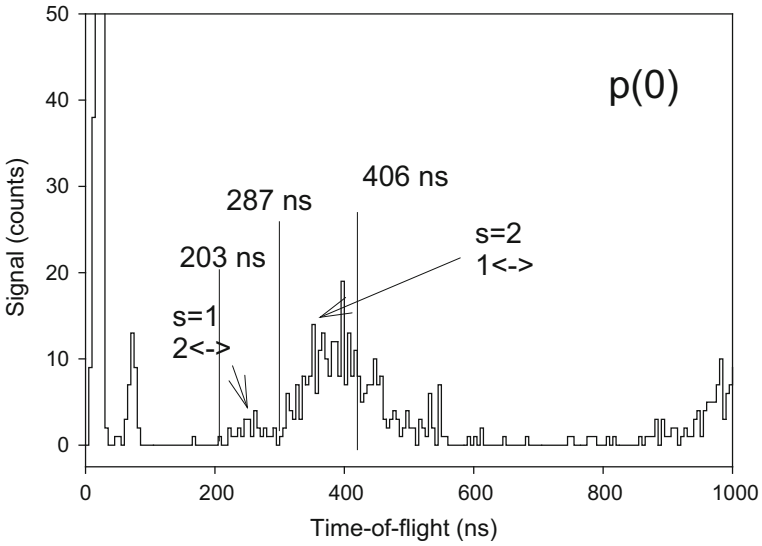

Fig. 10 Neutral MCS spectrum for fragmentation of small p($l = 0$) clusters, using the setup in Fig. 3(a). Laser at end face of magnet, inner detector, 1,000 shots. TOF limits indicated are given in Table 3

Table 2 Symmetric fragmentation of p($l = 0$) **clusters with flight times** t **in the present experiments**

Total cluster charge	Total cluster mass	Name [4]	Inner detector t (ns)	Outer detector t (s)	In Fig. no.
4+	4	4(CE4+)S	237	2.6	
3+	3	3(CE3+)S	291	3.2	
2+	20	10←→10	1,301	14.4	
2+	18	9←→9	1,234	13.7	
2+	16	8←→8	1,163	12.9	
2+	14	7←→7	1,088	12.1	11
2+	12	6←→6	1,007	11.2	
2+	10	5←→5	920	10.2	11
2+	8	4←→4	823	9.1	
2+	6	3←→3	712	7.9	
2+	4	2←→2	582	6.5	
2+	2	1←→1	411	4.6	

The 2+ charge CE processes give energy 315 eV to each of the two fragments

degrees of freedom and their rotational spectra for clusters $K_N(l)$ have been studied and interpreted in detail [25, 26]. The magnetic dipoles are fixed in the clusters and will rotate (by precession) in space around the direction of the magnetic field [27], but with further effects due to the thermal motion of the clusters [25, 26]. This

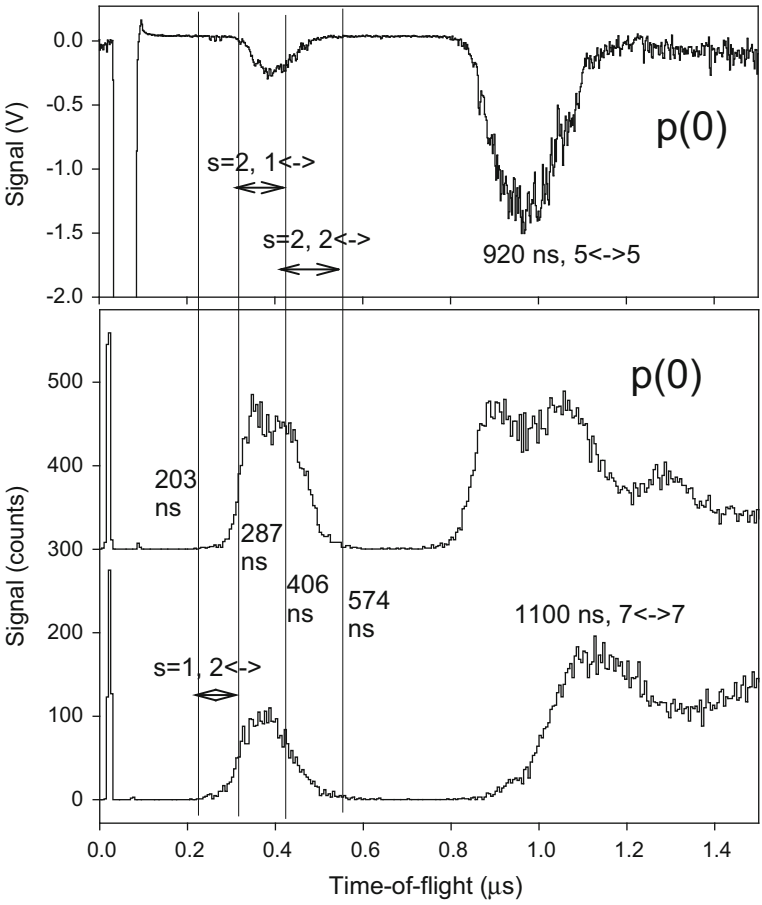

Fig. 11 MCS (*bottom panel*) and oscilloscope (*top panel*) spectra of small neutral p($l = 0$) clusters, using the setup in Fig. 3(a). Side face of magnet, inner detector, 500 shots in the MCS spectra. 512 shots in oscilloscope averaging. TOF limits indicated are from Table 3

Table 3 Time-of-flight limits for fragmentation of small p($l =$ **0) clusters to the inner detector at 101 mm**

Spin level for p($l = 0$)	Ejected p		Ejected p_2	
	$p^+ \longleftrightarrow p_N^+$	$p^+ \longleftrightarrow p^+$	$p_2^+ \longleftrightarrow p_N^+$	$p_2^+ \longleftrightarrow p_2^+$
$s = 1$	(144 ns)	(203 ns)	203 ns	287 ns
$s = 2$	287 ns	406 ns	406 ns	574 ns

Ejection of protons p and proton pairs p_2 are both included, for spin levels $s = 1$ and 2 [7]. The limits given are also indicated in Figs. 10 and 11. The limits within parentheses are not observed in the experiments

means that it is unlikely that a substantial line-up of the magnetic dipoles will take place to give a behavior similar to superconductivity. Effects of this type would be most easily observed for clusters p(3) and p(4) where planar forms dominate [21]. For example p(1) gives more complex 3-dimensional forms [28, 29] even in cases where p(0) is not formed easily. In Fig. 4, higher RM states should be observed at TOF longer than 10 s. The intensity above the magnet pole face in this TOF range is lower than for the other spectra in Fig. 4. (The spectra were indeed measured up to 90 s but with no signal increase above the magnet). Thus, the planar RM clusters p (3) and p(4) do not show a Meissner effect, as expected from the nature of the cluster rotation. A pure diamagnetic effect is believed to not be strong in the planar clusters with strong dipoles, but may be more important for larger clouds of RM.

Thus, the main results are that p(0) clusters behave similar to D(0) clusters in a magnetic field, but that the Meissner effect is smaller in p(0) due to the less than perfect symmetry of the cluster shapes. Another property where the difference is even larger between p(0) and D(0) is the structure of the small clusters observed not to float in the magnetic field in the case of D(0). These clusters are mainly of the type $D_4(0)$, assumed to have tetrahedron form or at least two symmetric pairs D_2 connected to each other. Signal was also observed [6] corresponding to D_3 clusters, which are assumed to be symmetric planar clusters. The TOF spectra corresponding to such clusters have been calculated and analyzed in detail [4], with the result that the most common form is D_4. This gives a symmetric fragmentation named 8(4+)S, where the 4+ indicates the charge of the cluster breaking up in the CE process, not of the fragments which are singly charged. For clarity, we here add CE to indicate this, as in 8(CE4+)S. For D_3, this symmetric fragmentation is then named 6(CE3+) S. The corresponding clusters p_4 and p_3 should fragment according to specifications 4(CE4+)S and 3(CE3+)S with TOF values given in Table 2. A comparison of these values with Figs. 10 and 11 gives only a partial explanation. For example, in Fig. 10 no maximum is observed at the position for the p_3 cluster fragmentation at 291 ns [3 (CE3+)S in Table 2] contrary to expectation. The fast rise of the signal and the main intensity in Figs. 10 and 11 are not described by either p_4 or p_3 fragmentation. Thus, only low intensities of such clusters are observed on the magnet surfaces in Figs. 10 and 11, and almost none on the magnet pole face in Figs. 4, 5, 6 and 7. It is certainly difficult to understand from a fundamental point of view how a cluster p_4 could exist at all. Two protons may pair with the proton ½ spins in opposite directions giving bosons (seen at long distance), but cramping two such bosons together to form a p_4 entity may be difficult. Further, if the shape of p_4 would be analogous to D_4, all the protons need to be symmetrically arranged which appears impossible. The extensive laser fragmentation results from $p(l = 0)$ [16] show clearly that p_2 pairs are formed, probably mainly at the end positions in the chain clusters, but they mainly pair up with single protons p in the chain structure giving the special mode of fragmentation $p_2^+ \longleftrightarrow p+$ explained in Ref. [16]. Thus, no symmetric small clusters are expected or observed for $p(l = 0)$.

Instead, the results in Figs. 10 and 11 may be analyzed using the theoretical development of the different spin states in $H(l = 0)$ given in [7]. The result is that good agreement is found with processes ejecting both p and p_2 from clusters with spin levels $s = 1$ and 2, as given in detail in Table 3. According to Table 3, no

intensity is found for the process ejecting p from the spin level $s = 1$, while the similar process from spin level $s = 2$ is observed. This may be due to the very short distance of 0.57 pm in level $s = 1$, which is likely to give either pairing to p_2 or strong repulsion. Thus, $s = 1$ may be possible only for proton pairs, not giving symmetric p_4 entities but only two bosons p_2 at close distance. Certainly, the intensity for such processes is low both in Figs. 10 and 11. It is further possible that the process giving the low signal starting at 203 ns in the spectra is not due to p_2 pairs at all but to D atoms. A few D atoms exist at a fractional concentration of 1.6×10^{-4} in the natural hydrogen H_2 gas used. Thus, the fragmentation giving the small signal between 203 and 287 ns in Figs. 10 and 11 could be $D^+ \longleftrightarrow p_N^+$ instead of $p_2^+ \longleftrightarrow p_N^+$ as assumed in Table 3. Thus, the spin level $s = 1$ for p($l = 0$) is not observed with confidence and may indeed be difficult to identify without using pure protium gas.

Conclusions

A Meissner effect is detected from the lifting of clusters of spin level $s = 2$ of ultra-dense protium p($l = 0$) in a static magnetic field, sampling the cluster cloud with a laser beam. This indicates that p($l = 0$) is superconductive. The Meissner effect in p ($l = 0$) is weaker than in ultra-dense deuterium D($l = 0$), which has been studied previously. This is proposed to be due to the more complex structure of the $p_N(l = 0)$ clusters. No small symmetric clusters of p($l = 0$) are found that do not lift in the magnetic field, contrary to the case of D($l = 0$) where such clusters stayed at the magnet pole face. The signal due to small clusters of p($l = 0$) partly corresponds to ejection of p_2 pairs, which supports the previous identification of such pairs in p ($l = 0$).

References

1. S. Badiei, P. U. Andersson, and L. Holmlid (2010). *Phys. Scr.* **81**, 045601.
2. S. Badiei, P. U. Andersson, and L. Holmlid (2010). *Appl. Phys. Lett.* **96**, 124103.
3. P. U. Andersson, B. Lönn, and L. Holmlid (2011). *Rev. Sci. Instrum.* **82**, 013503.
4. L. Holmlid (2011). *Int. J. Mass Spectrom.* **304**, 51.
5. P. U. Andersson and L. Holmlid (2011). *Phys. Lett. A* **375**, 1344.
6. P. U. Andersson, L. Holmlid, and S. R. Fuelling (2012). *J. Supercond. Novel Magn.* **25**, 873.
7. L. Holmlid (2013). *Int. J. Mass Spectrom.* **352**, 1.
8. L. Berezhiani, G. Gabadadze, and D. Pirtskhalava (2010). *J. High Energy Phys.* **4**, 122.
9. P. U. Andersson and L. Holmlid (2012). *Int. J. Mass Spectrom.* **310**, 32.
10. P. U. Andersson and L. Holmlid (2012). *Phys. Scr.* **86**, 045601.
11. F. Winterberg (2010). *J. Fusion Energy* **29**, 317.
12. F. Winterberg (2010). *Phys. Lett. A* **374**, 2766.
13. T. Guénault *Basic Superfluids* (Taylor & Francis, London, 2003).
14. F. Olofson and L. Holmlid (2012). *J. Appl. Phys.* **111**, 123502.
15. F. Olofson and L. Holmlid (2012). *Nucl. Instr. Method B* **278**, 34.
16. L. Holmlid (2013). *Int. J. Mass Spectrom.* **351**, 61.
17. E. A. Manykin, M. I. Ojovan, and P. P. Poluektov (2006). *Proc. SPIE* **6181**, 618105.
18. É. A. Manykin, M. I. Ozhovan, and P. P. Poluéktov (1992). *Sov. Phys. JETP* **75**, 440.
19. L. Holmlid (1998). *Chem. Phys.* **237**, 11.

20. L. Holmlid (2012). *J. Cluster Sci.* **23**, 5.
21. L. Holmlid (2012). *J. Clust. Sci.* **23**, 95.
22. J. E. Hirsch (2010). *Physica C* **470**, 635.
23. G. R. Meima and P. G. Menon (2001). *Appl. Catal. A* **212**, 239.
24. M. Muhler, R. Schlögl, and G. Ertl (1992). *J. Catal.* **138**, 413.
25. L. Holmlid (2007). *Mol. Phys.* **105**, 933.
26. L. Holmlid (2008). *J. Mol. Struct.* **885**, 122.
27. H. Haken and H. C. Wolf *The Physics of Atoms and Quanta*, 7th ed (Springer, Berlin, 2005).
28. L. Holmlid (2008). *Surf. Sci.* **602**, 3381.
29. L. Holmlid (2011). *J. Nanopart. Res.* **13**, 5535.